PAPER

Scaling of the tokamak near the scrape-off layer H-mode power width and implications for ITER

To cite this article: T. Eich *et al* 2013 *Nucl. Fusion* **53** 093031

Nucl. Fusion **53** (2013) 093031 (7pp) doi:10.1088/0029-5515/53/9/093031

Scaling of the tokamak near the scrape-off layer H-mode power width and implications for ITER

T. Eich[1], A.W. Leonard[2], R.A. Pitts[3], W. Fundamenski[4], R.J. Goldston[5], T.K. Gray[6], A. Herrmann[1], A. Kirk[4], A. Kallenbach[1], O. Kardaun[1], A.S. Kukushkin[3], B. LaBombard[7], R. Maingi[5,6], M.A. Makowski[8], A. Scarabosio[1], B. Sieglin[1], J. Terry[7], A. Thornton[4] and ASDEX Upgrade Team and JET EFDA Contributors[a]

JET-EFDA, Culham Science Centre, Abingdon, OX14 3DB, UK
[1] Max-Planck-Institut für Plasma Physik, Boltzmannstr.2, 85748 Garching, Germany
[2] General Atomics, PO Box 85608, San Diego, CA 92186-5608, USA
[3] ITER Organization, Route de Vinon sur Verdon, 13115 Saint Paul Lez Durance, France
[4] CCFE, EURATOM-Association, Culham Science Centre, Abingdon, UK
[5] Princeton, Plasma Physics Laboratory, Princeton, NJ 08543, USA
[6] Oak Ridge National Laboratory, Oak Ridge, TN 37831, USA
[7] MIT Plasma Science and Fusion Center, Cambridge, MA 02139, USA
[8] Lawrence Livermore National Laboratory, Livermore, CA 94551, USA

Received 11 March 2013, accepted for publication 9 August 2013
Published 29 August 2013
Online at stacks.iop.org/NF/53/093031

Abstract
A multi-machine database for the H-mode scrape-off layer power fall-off length, λ_q in JET, DIII-D, ASDEX Upgrade, C-Mod, NSTX and MAST has been assembled under the auspices of the International Tokamak Physics Activity. Regression inside the database finds that the most important scaling parameter is the poloidal magnetic field (or equivalently the plasma current), with λ_q decreasing linearly with increasing B_{pol}. For the conventional aspect ratio tokamaks, the regression finds $\lambda_q \propto B_{\mathrm{tor}}^{-0.8} \cdot q_{95}^{1.1} \cdot P_{\mathrm{SOL}}^{0.1} \cdot R_{\mathrm{geo}}^{0}$, yielding $\lambda_{q,\mathrm{ITER}} \cong 1$ mm for the baseline inductive H-mode burning plasma scenario at $I_{\mathrm{p}} = 15$ MA. The experimental divertor target heat flux profile data, from which λ_q is derived, also yield a divertor power spreading factor (S) which, together with λ_q, allows an integral power decay length on the target to be estimated. There are no differences in the λ_q scaling obtained from all-metal or carbon dominated machines and the inclusion of spherical tokamaks has no significant influence on the regression parameters. Comparison of the measured λ_q with the values expected from a recently published heuristic drift based model shows satisfactory agreement for all tokamaks.

(Some figures may appear in colour only in the online journal)

1. Introduction

Operation in a diverted H-mode plasma is fundamental to the achievement of high fusion gain in ITER. Most of the $P_{\mathrm{SOL}} \sim 100$ MW of power crossing the separatrix at $Q_{\mathrm{DT}} = 10$ in ITER must flow inside a narrow channel on open field lines in the scrape-off layer (SOL) connecting directly to the divertor target plates. The most appropriate scaling for the width, λ_q, of this heat flux channel is still under discussion. Based mostly on JET ELM-averaged data, the ITER Physics basis [1] concluded $\lambda_q \sim 3$–3.5 mm for $Q_{\mathrm{DT}} = 10$, close to the value adopted in ITER plasma boundary modelling [2]. Recent results, reported here, obtained through a multi-machine coordinated effort (JET, DIII-D, ASDEX Upgrade (AUG), C-Mod, NSTX and MAST) conducted in part through the International Tokamak Physics Activity Divertor and SOL Topical Group, indicate that this assumed ITER value is too large. Scaling from the new database provides a very clear dependence on the poloidal magnetic field, minor variation with other key variables, and suggests $\lambda_q \cong 1$ mm for ITER.

[a] See the appendix of Romanelli F. *et al* 2012 *Proc. 24th IAEA Fusion Energy Conf. 2012 (San Diego, CA, 2012)* www-naweb.iaea.org/napc/physics/FEC/FEC2012/papers/197_OV13.pdf.

2. Experimental estimation of the power fall-off width and power spreading factor

To a large extent, the new findings reported here have been obtained through significant improvements in both analysis and the spatio-temporal resolution of the infra-red (IR) thermography diagnostics that are now standard on many tokamaks for divertor target heat flux measurements. To collect the data, these cameras were employed to measure the inter-ELM heat flux footprint over a wide range of heating power on the outer divertor targets of attached, low radiating H-mode discharges with carbon plasma-facing components (PFCs) except for C-Mod which has a full metal wall and divertor. The use of such discharges is of primary importance for these studies, which seek to find a scaling of the inter-ELM SOL power width adjacent to the main plasma far upstream of the divertor. In this case, the complexity of partially detached divertor plasmas must be avoided if a measurement at the target plate is to be meaningfully extrapolated back up-stream. The outer target is a naturally easier place to make these measurements since, for forward toroidal field direction (the standard direction used on most tokamaks, including ITER), the inter-ELM heat flux is always higher on the outer target in comparison with the inner [3–5]. As a result, the inner target is more easily in a partially detached condition. On ITER, in fact, power handling constraints mean that partial detachment will be required at both divertor strike points (a point to which section 6 will return).

Other key improvements in data analysis are (1) the avoidance of ELM effects and (2) accounting for changes in the target deposition profile due to heat diffusion across the divertor legs into the private flux region [6, 7]. Experimentally, almost the complete operational range of plasma current and toroidal field in each device was scanned. The analysis of measured divertor target profiles in the outer divertor of each machine follows the approach introduced in [6] which is summarized in the remainder of this section.

Assuming a purely exponential radial decay (characterized by λ_q) of the parallel energy transport, the inter-ELM outboard midplane SOL parallel heat flux profile can be written as $q(r) = q_{\parallel} \cdot \mathrm{e}^{-r/\lambda_q}$, where $r = R - R_{\mathrm{sep}}$, R_{sep} being the major radius of the separatrix at the outer midplane. We further assume that λ_q is dependent only on the upstream outer midplane SOL parameters and the magnetic connection length along field lines to the outer target, L_{c}. Heat transport into the private flux region is included by describing the observed power spreading (diffusion/dissipation) along the divertor leg between the X-point and the target as a Gaussian spreading of a point heat source; this can simply be taken into account by convoluting $q(r)$ with a Gaussian function of width S [10], which we refer to as the *power spreading parameter* and which is assumed to be dependent on local divertor plasma parameters and geometry. The result of this convolution is the following expression for the outer target profile [6]:

$$q(\bar{s}) = \frac{q_0}{2} \cdot \exp\left(\left(\frac{S}{2\lambda_q}\right)^2 - \frac{\bar{s}}{\lambda_q \cdot f_x}\right) \cdot \mathrm{erf}c\left(\frac{S}{2\lambda_q} - \frac{\bar{s}}{S \cdot f_x}\right) + q_{\mathrm{BG}} \quad \text{and} \quad \bar{s} = s - s_0 = (R_{\mathrm{sep}} - R) \cdot f_x. \tag{1}$$

The other quantities used in equation (1) are the background heat flux, q_{BG}, the effective flux expansion, f_x, on the target following the definition in [9], and the peak heat flux at the divertor entrance $q_{\parallel} = q_0/\sin(\theta_{\perp})$ with $\theta_{\perp}$ the field line angle on the divertor target. Typical profiles measured at the divertor targets and fitted with equation (1) are shown in figure 1 for each of the participating devices. For AUG the pure exponential profile is added for reference. In the common flux (main divertor SOL) region, the profiles closely follow an exponential decay and heat is clearly also transported into the private flux region. The profile can be well described by numerical least-squares fits according to equation (1) for all cases.

A quantity of interest is the so called *integral power decay length,* relating the peak heat flux and the deposited power and defined as $\lambda_{\mathrm{int}} = \int (q(r) - q_{\mathrm{BG}})\,\mathrm{d}r'/q_{\mathrm{max}}$ [9], where q_{max} is the measured peak heat flux on the target. As shown by Makowski [7], $\lambda_{\mathrm{int}} \cong \lambda_q + 1.64 \cdot S$ is satisfied to a good approximation (error <4% for $S/\lambda_q < 10$) when equation (1) gives a reasonable fit to the experimental data. With this finding in mind, it is clear that a regression of λ_q describing upstream transport cannot be substituted by a regression on λ_{int}, as used in earlier attempts [8, 9]. Instead, λ_q and S are analysed separately. Since S includes geometrical effects of the divertor assembly itself, (see section 5), an extrapolation of S to ITER is not envisaged in this contribution. We focus on the regression of λ_q as input for characterization of the ITER SOL, and use equation (1) for its derivation throughout.

3. Discharge database

Table 1 provides an overview of the important plasma and machine parameters for the multi-machine, outer target λ_q database. It should be noted that although the paper focuses on inter-ELM transport, only JET, DIII-D, AUG and MAST [16] provide data that is strictly taken from inter-ELM time windows. Data from C-Mod have been obtained in ELM-free EDA H-mode [12]. For NSTX, large ELMs are removed from the IR data, but smaller transient events are still included. The definitions of the various parameters in table 1 are, I_{plasma} for plasma current, B_{tor} for toroidal magnetic field, q_{95} for the safety factor at the 95% poloidal flux surface, P_{sol} for the power crossing the separatrix, A_{sep} the separatrix surface, B_{pol} for the poloidal magnetic field at the outer midplane separatrix, n_{GW} for the Greenwald density fraction, R_{geo} for major radius, a for minor radius, δ for triangularity and κ for elongation.

4. Regression results

The following regressions are chosen to compare with already published material from the single devices or working groups and do not reflect a rigorous treatment of all possible choices of combining or ignoring individual parameters and devices. A Student t-test on typical independent parameters for tokamak operation is shown at the end of this section.

We first focus on regression of power widths obtained in conventional tokamaks operating in type I ELMy H-mode and for which the data allow clear isolation of inter-ELM outer target heat flux profiles: JET, DIII-D and AUG. In the case of JET and AUG, these inter-ELM periods cover 50–99% of the

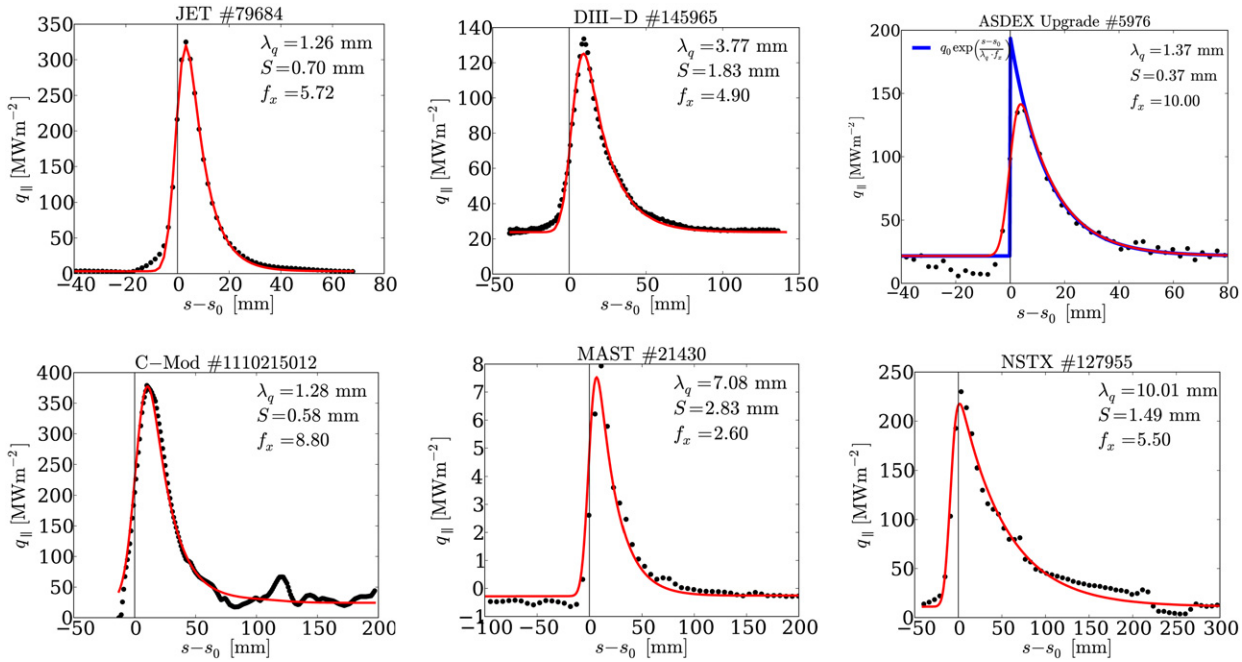

Figure 1. Typical outer target power parallel heat flux for each machine and result of fitting equation (1).

Table 1. Overview of parameter range for each device as used for regression.

	I_{plasma}	B_{tor}	q_{95}	P_{SOL}	P_{SOL}/A_{sep}	B_{pol}	n_{GW}	R_{geo}	a	δ	κ
Unit	MA	T	—	MW	MW m^{-2}	T	—	m	m	—	—
JET	1.0–3.5	1.1–3.2	2.6–5.5	2–12	0.01–0.09	0.2–0.7	0.4–0.9	2.95	0.95	0.2–0.4	1.8
DIII-D	0.7–1.5	1.2–2.2	3.2–7.3	1–5	0.02–0.09	0.2–0.5	0.4–0.7	1.74	0.51	0.2–0.4	1.8
AUG	0.8–1.2	1.9–2.4	2.6–5.1	2–5	0.06–0.19	0.2–0.5	0.4–0.7	1.65	0.51	0.1–0.3	1.7
C-Mod	0.5–0.9	4.6–6.2	3.8–6.6	1–3	0.13–0.36	0.5–0.8	0.5–0.7	0.7	0.22	0.3–0.4	1.6
NSTX	0.6–1.2	0.4–0.5	5.5–9.0	2–6	0.08–0.19	0.2–0.3	0.5–1.1	0.87	0.60	0.4–0.6	2.1
MAST	0.4–1.0	0.4	4.9–6.8	1–5	0.05–0.18	0.1–0.2	0.3–0.6	0.87	0.61	0.4–0.5	1.8
ITER	15	5.3	3	100	0.147	1.185	0.85	6.2	2.0	0.44	1.8

ELM cycle and for DIII-D, 30–99%. All data are taken by fast framing IR systems with typical sample times of 10 kHz, and hence fully resolve the ELM cycle. We use the plasma and machine parameters summarized in table 1 and employ standard numerical tools for regression, using power laws with a constant denoted as C such that $\lambda_q = C \times X^x Y^y Z^z$, etc, with R^2 the multiple (squared) correlation coefficient. The data was fitted on normal scale. We subsequently add data from C-Mod since this device operates in ELM-free H-mode. The results may be summarized as follows, referring to table 2 for the 'regression number'.

Regressions 1–3: the poloidal magnetic field, B_{pol} ($\sim I_{plasma}/a$) at the outer midplane is identified as a strong driver for a narrowing of the power fall-off length. This result has been found separately on all devices in earlier studies [7, 8, 12–16]. Regression in the database finds a linear inverse dependency on I_{plasma} and an approximately linear dependence on the minor radius, as expected. We attribute the slight deviation of the minor radius dependence to effects associated with the exact magnetic geometry, such as elongation, Shafranov shift, and triangularity. Adding C-Mod data does not lead to any notable differences.

Regressions 4–5: since the connection length is an important parameter for the parallel SOL transport, we add q_{95} as a proxy for the actual SOL connection length ($L_c \sim \pi R q_{95}$) and also explicitly include the machine size. Most notably, no dependence on the latter is found. As before, B_{pol} shows the strongest dependence, but is accompanied by a minor positive dependence of λ_q on q_{95}. Again the inclusion of C-Mod data does not change the results within the error bars of the regression parameters.

Regressions 6–9: we next use the B_{tor}, q_{95}, P_{SOL} and R_{geo} of each device. The latter choice follows the work in [8, 12] here focussing on identifying machine size dependency and on P_{SOL}. A strong positive dependence on P_{SOL} would be very beneficial for ITER, for which $P_{SOL} \sim 100$ MW for the $Q = 10$ baseline inductive scenario, about 20 times higher than the values typically found in the database of current tokamaks. Regression #6 gives results for JET only, DIII-D, AUG and finally C-Mod data being added consecutively for regressions #7–9. When comparing results from #6 to #9 the regression parameters found are essentially unchanged, which may be noted as an important intermediate step. The dependence on P_{SOL} is found to be weak but positive for the hierarchically ordered combinations of JET/DIII-D/AUG/C-Mod. The main parametric dependencies found are an almost linear variation with q_{95} and a strong inverse dependence on B_{tor}.

Since ITER will run its baseline H-mode with similar q_{95} ($\sim$3) to current devices, but at about twice the toroidal field

Table 2. Overview of selected regression results for tokamaks JET, DIII-D, AUG, C-Mod.

	#	C	B_{tor}	q_{95}	P_{Sol}	R_{geo}	I_{plasma}	a	B_{pol}	n/n_{GW}	R^2
Unit	—	mm	T	—	MW	m	MA	m	T	—	—
JET/DIII-D/AUG	1	0.68	—	—	—	—	—	—	−1.07	—	0.68
JET/DIII-D/AUG	2	3.60	—	—	—	—	−1.00	0.83	—	—	0.69
JET/DIII-D/AUG/C-Mod	3	0.65	—	—	—	—	—	—	−1.11	—	0.76
JET/DIII-D/AUG	4	0.61	—	0.30	—	0.00	—	—	−0.78	—	0.77
JET/DIII-D/AUG/C-Mod	5	0.52	—	0.25	—	0.10	—	—	−0.92	—	0.77
JET	6	0.40	−0.82	1.42	0.15	—	—	—	—	—	0.65
JET/DIII-D	7	0.67	−0.71	1.03	0.05	0.08	—	—	—	—	0.70
JET/DIII-D/AUG	8	0.74	−0.71	1.01	0.09	−0.05	—	—	—	—	0.69
JET/DIII-D/AUG/C-Mod	9	0.70	−0.77	1.05	0.09	0.00	—	—	—	—	0.77
JET/DIII-D/AUG	10	0.49	−0.69	0.95	0.05	0.29	—	—	—	−0.55	0.74
JET/DIII-D/AUG/C-Mod	11	0.52	−0.63	0.95	0.05	0.21	—	—	—	−0.48	0.80
JET/DIII-D/AUG (restr.)	12	1.59	(P_{Sol}/A_{sep})^0.44			0.38	—	—	−1.12	—	0.62

(5.3 T), values at the lower end of all observed data in the present devices in the range of $\lambda_q \sim 1$ mm are found when extrapolating today's tokamak results to ITER. For example, when using regressions #7–9 $\lambda_{q,ITER} = 0.9 \pm 0.2$ mm is found.

Regressions 10–11: the Greenwald density fraction, n_{GW} is added as a further parameter in the regression. Here, n_{GW} acts a proxy for the separatrix density, which is the real density of interest for scaling λ_q, but which is not measured with sufficient precision in most devices due to uncertainties in the separatrix location obtained from magnetic reconstruction, or simply in the absence of a suitable diagnostic. Unfortunately, n_{GW} is a strong function of machine size and thus introduces covariance with R. Keeping this caveat in mind, we see that regressions #10 and #11 find a positive dependence on R_{geo} and an approximately inverse square root dependence on n_{GW}. Inclusion of n_{GW} does not change the value of $\lambda_{q,ITER} \cong 1$ mm obtained from the previous regression attempts.

Figure 2 (left) illustrates the results of regression #9. Here it is interesting to note that the database from each device includes values of $\lambda_q \sim 1.5$ mm. In particular the largest (JET) and the smallest (C-Mod) device databases, contain measured values of $\lambda_q \sim 1$ mm at high I_{plasma}. Hence, the extrapolated value for ITER is in the range of outer midplane power decay lengths measured in current tokamaks, and notably in devices at each extremity of the size scale, supporting the absence of a machine size dependency. In addition, figure 1 shows that similar parallel heat flux densities $q_{\|} \sim 300\,\mathrm{MW\,m^{-2}}$ are observed in both JET and C-Mod. We note for completeness, that the largest values of the parallel heat flux are those from strongly heated (20 MW) and high current (3.5 MA) JET discharges, in which $q_{||}$ can reach $600\,\mathrm{MW\,m^{-2}}$.

Regression 12: an important goal of the multi-machine database is to examine the dependency of λ_q on machine size (R_{geo}), something which cannot be obtained from a single device; a factor of 4 variation of R_{geo} is represented here. However, from table 1 we note that the heat flux density crossing the separatrix (P_{SOL}/A_{sep}) decreases systematically with machine size. The covariance between these parameters does not allow us to fully separate potential dependencies on R_{geo} and P_{Sol}/A_{sep} over the full dataset. Indeed, a restricted dataset involving JET, D3D and AUG with $0.05 < P_{SOL}/A_{sep} < 0.1$ suggests that λ_q may exhibit a scaling with R_{geo} that is offset by a scaling with P_{SOL}/A_{sep}. The extrapolated value when using regression #12 gives $\lambda_{q,ITER} = 1.1$ mm.

Table 3. Regression results including MAST and NSTX.

	#	C	P_{SOL}	R_{geo}	B_{pol}	a/R_{geo}	R^2
Unit	—	mm	MW	m	T	—	—
MAST/ NSTX	13	1.22	—	—	−0.84	—	0.40
All	14	0.63	—	—	−1.19	—	0.86
All	15	1.35	−0.02	0.04	−0.92	0.42	0.88

Regressions 13–15: both NSTX and MAST are spherical tokamaks with an aspect ratio of 0.69, which is about twice the value of that for the conventional tokamaks in the database. We first compare the scaling results of these two devices separately and then combine them with the other four machines with the main aim being to elucidate any dependence on a/R_{geo}. Table 3 gives an overview of the parametric dependencies found using the same scaling hierarchy as in the previous section. Regression #13 on combined MAST and NSTX data recovers the previous result seen for the conventional aspect ratio tokamaks: the measured λ_q decreases approximately linearly with increasing B_{pol}. The regression quality is reduced in comparison with those found in table 2, due to a higher average scatter in the spherical tokamak data. Extending the regression to all devices, the inverse scaling of λ_q with B_{pol} alone orders the data reasonably well, as might be expected given the dependence found separately for the two tokamak groups (regression #14).

The combined scaling of all devices in regression #15 (figure 2 right) gives a value for ITER close to the one found in the previous section for all conventional tokamaks and results in $\lambda_{q,ITER} = 0.73$ mm. As before, there is no major radius scaling, but the regression identifies a strong dependence on the aspect ratio: $(a/R)^{0.4}$. If the regressions with B_{pol} or those using combined I_{plasma} and a as the sole scaling parameter (regressions #1,2,3 and #13) are used to extrapolate to ITER, slightly lower values in the range $\lambda_{q,ITER} = 0.6$ mm are found. In addition, regressions #4,5,14,15 yield $\lambda_{q,ITER} < 1$ mm due to the absence of the slight positive P_{SOL} scaling (since $P_{SOL,ITER}/P^{0.1}_{SOL,\langle ALL\rangle} = 22^{0.1} = 1.36$ with $P_{SOL,\langle ALL\rangle}$ as the mean value for data base).

Student t-test: here we return to the introductory statement of this paragraph and focus on results of applying Student t-tests to select regression variables for the presented data set. Again, this work could be further extended by making use

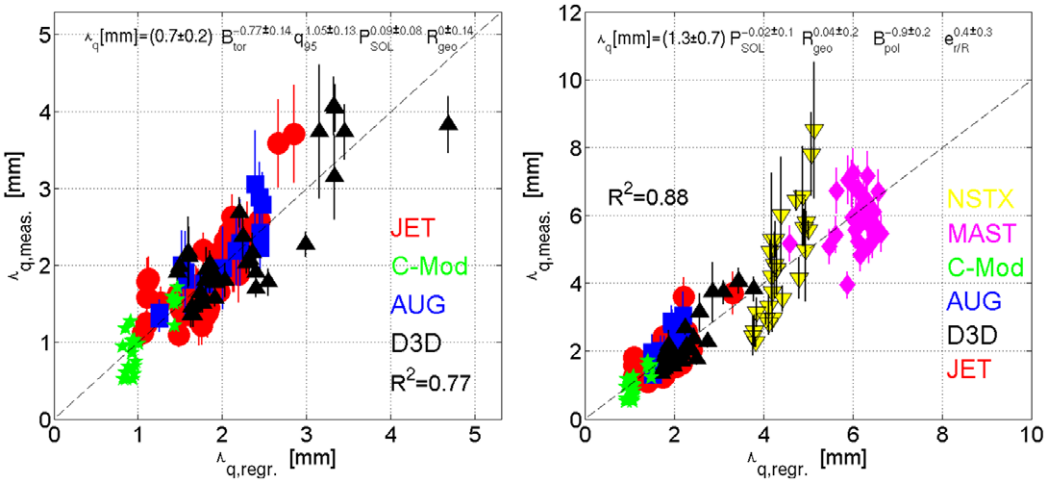

Figure 2. Results from (left) regression #9 and (right) regression #15.

Table 4. Variable selection based on performing univariate consecutive t-tests.

Device	B_{tor} (T)	P_{SOL} (MW)	R_{geo} (m)	B_{pol} (T)	n/n_{GW}	a/R_{geo}	R^2
All	0.07 ± 0.21	0.12 ± 0.12	-0.09 ± 0.18	-1.12 ± 0.19	0.01 ± 0.23	0.18 ± 0.49	0.89
All	0.01 ± 0.12	0.12 ± 0.11	-0.14 ± 0.13	-1.12 ± 0.19	0.03 ± 0.23	—	0.88
All	-0.12 ± 0.12	0.01 ± 0.12	-0.09 ± 0.15	-1.01 ± 0.19	—	—	0.87
All	-0.13 ± 0.11	—	-0.09 ± 0.11	-0.93 ± 0.16	—	—	0.87
All	-0.17 ± 0.09	—	—	-0.93 ± 0.16	—	—	0.87
All	—	—	—	-1.19 ± 0.08	—	—	0.86
J/D/A/C	0.33 ± 0.15	0.16 ± 0.08	0.13 ± 0.15	-1.27 ± 0.15	-0.48 ± 0.19	—	0.83
J/D/A/C	0.28 ± 0.14	0.20 ± 0.07	—	-1.31 ± 0.14	-0.38 ± 0.16	—	0.83
J/D/A	0.35 ± 0.18	0.16 ± 0.07	0.08 ± 0.21	-1.26 ± 0.16	-0.44 ± 0.24	—	0.78
J/D/A	0.35 ± 0.18	0.18 ± 0.07	—	-1.27 ± 0.15	-0.37 ± 0.17	—	0.78

of this statistical approach for different combinations of the participating devices, e.g. focusing only such devices with data obtained in type-I ELMy H-mode. As this would clearly be beyond the scope of the paper, we restrict the presented work to the discussed choice of various devices as presented in table 4.

The following independent scaling parameters SOL power (P_{SOL}), the Greenwald fraction (n_{GW}), the toroidal magnetic field (B_{tor}), the poloidal magnetic field at the outer midplane ($B_{pol,MP}$), the major radius (R_{geo}) and the aspect ratio (a/R_{geo}) are used simultaneously. Then all parameters that are statistically irrelevant i.e. are removed progressively. The order is chosen in such a way that the quantity having the largest relative error is removed first. This procedure is illustrated in table 4.

The result is that practically only the poloidal magnetic field is identified to be statistically important. We remind the reader that we intentionally did not remove the SOL power and the major radius from tables 2 and 3. The dependence of the power fall-off length on the latter two parameters was discussed intensely in the literature in the last decade as for a next step device both the SOL power and the major radius will be significantly larger. As shown in table 4, by removing the two spherical tokamaks (and then not including the aspect ratio as a regression parameter), the dependency on the Greenwald density fraction becomes additionally statistically relevant, also the toroidal field and SOL power, but again with practically very little influence. Removing the data from C-Mod, the only conventional device not operating in the type-I ELMy H-mode regime, does not lead to any changes as shown again in table 4.

The result of this procedure comes close to the result presented in regression #14. Notably a single parameter only, the poloidal magnetic field at the outer midplane ($B_{pol,MP}$), is sufficient to describe in practice (with a R^2 of 0.86) the entire database of all tokamaks including the spherical machines. However, at constant B_{pol}, B_{tor} seems to have some influence. The fair match between experimental data and the regression model is shown in figure 3. The graph describes the regression result (#14) and the error bars of the employed statistical regression model $\lambda_q\,(\mathrm{mm}) = (0.63 \pm 0.08) \times B_{pol,MP}^{-1.19\pm0.08}$.

Finally, we discuss the observed dependence on the Greenwald density fraction for the conventional tokamaks. Studies of L-mode plasmas in the far SOL revealed an increase of the SOL width with increasing Greenwald density fractions [26, 27]. The behaviour reported here shows the opposite trend, a narrowing of the power width with larger Greenwald density fractions. By the nature of multiple regression, this result has to be understood in our case as executed at constant B_{tor}, B_{pol}, P_{SOL} and R_{geo}.

As pointed out in the introduction section, the database focuses on attached divertor conditions achieved with very small gas puffing rates. A situation where the Greenwald density fraction is increased due to gas puffing in the SOL has to be strictly separated from a situation where the Greenwald density fraction is increasing due to changes of the particle confinement [28]. The underlying reason for this finding, however, certainly deserves close attention for future studies and refinement of this multi-machine database. A sensible

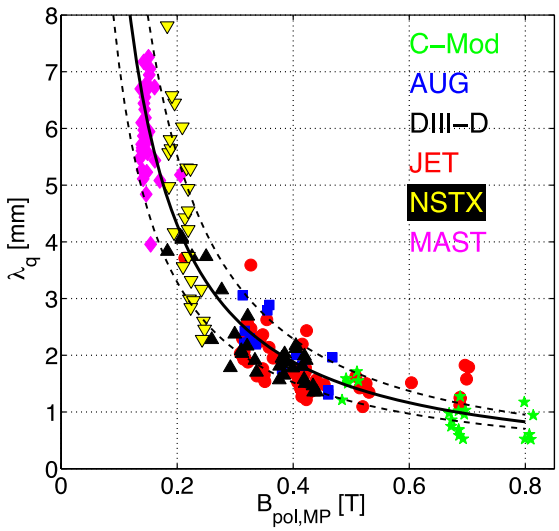

Figure 3. Poloidal magnetic field at the outer midplane versus power fall-off length (λ_q). The solid line gives the result of regression #14 and the dashed lines the error bars.

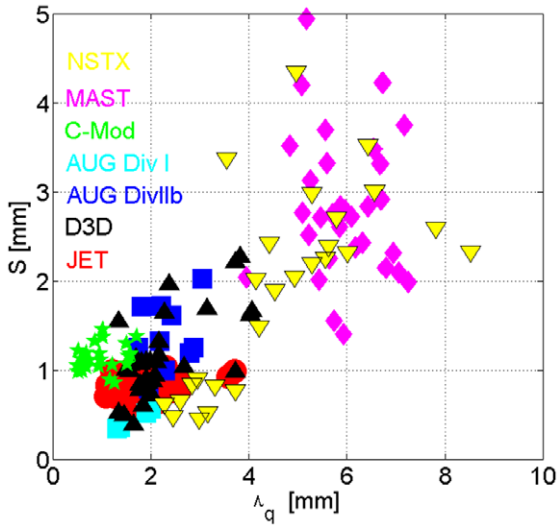

Figure 4. Comparison of power spreading factor (S) versus power fall-off length (λ_q).

strategy seems to employ the separatrix density as an additional parameter for scaling the power fall-off length. The extent to which the method of analysing target profiles for estimation of λ_q used here is suited in the presence of high gas puffing rates and edge densities, however, cannot be given yet.

5. Divertor power spreading value (S) from target profile fitting

Figure 4 plots the power spreading factor (S) versus λ_q for JET, DIII-D, AUG Divertor-I and Divertor-IIb and C-Mod. As shown in figure 4, JET, DIII-D and AUG cover the same range in λ_q of 1–4 mm. In contrast to this overlap of λ_q in the various conventional tokamaks, the values found for the power spreading factors appear to cluster around different mean values for each machine. In particular the different divertor geometries of AUG Divertor-I, with an open geometry (outer strike point on horizontal targets), and Divertor-IIb, with a relatively closed divertor geometry (outer strike point on vertical targets), have very different numerical values (table 5). Such a strong geometric dependence negates any attempt at scaling with global discharge parameter.

Recalling the approximation $\lambda_{\rm int} \cong \lambda_q + 1.64 \cdot S$ identified by Makowski [7], it becomes clear that a value of S larger than ∼1 mm would dominate over λ_q when determining $\lambda_{\rm int}$, and therefore an extrapolation of S to ITER is desirable, although estimates of $\lambda_{\rm int}$ for ITER would only apply for low SOL radiation, attached plasma conditions, which would not be tolerable at high performance from an engineering power handling point of view. We identify such an attempt, namely to estimate S for ITER conditions, as an important extension of this work. However the current database does not include parameters characterizing the divertor plasma conditions or geometry. Nevertheless, the comparison of AUG Divertor-I and Divertor-IIb, where the latter is similar to the closed ITER divertor geometry, suggests that S may give values of $\lambda_{\rm int}$ which exceed those observed for more open divertors. In this respect, we note that Divertor-IIb gives a factor of 3 in the power spreading factor in comparison with Divertor-I, which is a considerable improvement. We note, however, that the DIII-D values of S are similar to those of AUG Divertor-IIb which, given the very different divertor geometries between the two machines (of very similar scale size), will merit close attention when extending our approach towards a possible multi-machine based regression of S and hence to $\lambda_{\rm int}$.

6. Conclusions and implication for ITER

Regression in a multi-machine database (JET, DIII-D, AUG, C-Mod) for the SOL power width measured using outer divertor target IR thermography in low recycling H-mode discharges finds $\lambda_{q,\rm ITER} \cong 0.7$–$1.1$ mm for the baseline 15 MA, $Q = 10$ inductive H-mode burning plasma discharge. This range of extrapolated values overlaps the measured λ_q on JET and C-Mod, respectively the largest and smallest devices in the database, and is a rather clear demonstration of the absence of any detectable machine size scaling in the regression. Instead, the strongest and essentially only dependence amongst the regression variables tested, at least for the conventional aspect ratio tokamaks, is an inverse scaling with plasma current (or equivalently a linear dependence on outboard midplane poloidal magnetic field).

Recent studies in the JET ITER-Like Wall and full-W AUG [15] confirm the regression results, i.e. a high-Z 'tungsten' divertor environment has no effect on measured power fall-off width. This is of course already implicitly suggested by the database used here, which includes points from C-Mod running with high-Z metal PFCs (molybdenum).

The data obtained from earlier JET/AUG [6, 15] and DIII-D/C-Mod/NSTX [7, 14] studies are consistent in absolute magnitude with the predictions of a recently formulated heuristic drift-based theory [17]. Combining the data sets and adding the new MAST [16] data yields no notable deviation from these earlier findings (table 6). We find identical parametric dependences within error bars for all data recorded in type-I ELMy H-mode of the conventional tokamaks JET/DIII-D/AUG. The derived experimental and

Table 5. Variation of mean power spreading factor, S and S/λ_q for the various devices.

	JET	DIII-D	AUG DivI	AUG DivII	C-Mod	MAST	NSTX
S (mm)	0.59–1.04	0.39–2.27	0.35–0.56	0.79–2.02	0.86–1.46	1.11–4.95	0.46–4.35
$S\lambda_q$	0.26–0.81	0.24–1.14	0.26–0.28	0.40–0.94	0.67–2.32	0.17–0.95	0.15–0.95

Table 6. Comparison of regression results to Goldston heuristic-drift (HD) prediction.

	C (mm)	B_{tor}	q_{cyl}	P_{sol}	R_{geo}	R^2
JET/DIII-D/AUG	0.86 ± 0.25	-0.80 ± 0.21	1.11 ± 0.15	0.11 ± 0.09	-0.13 ± 0.16	0.71
Goldston HD	0.93 ± 0.06	-0.875	1.125	0.125	0	0.63

theoretical scalings yield $\lambda_{q,\mathrm{ITER}} \cong 0.8$–$0.9$ mm for deuterium plasmas.

It is important to reiterate that the measurements used to establish the scaling come from ELM-free periods in attached divertor discharges over a limited range of operating parameters compared to conditions expected on ITER at high performance. This analysis does not exclude other physical effects which may constrain λ_q to larger values when scaling to ITER. A possible constraint on λ_q due to a finite SOL pedestal pressure gradient, first raised in [18], is currently a matter of intense discussion in the community [19, 20].

The values for $\lambda_{q,\mathrm{ITER}}$ reported here are about a factor 3 lower than the lowest predictions on the basis of earlier studies [1]. Such narrow power channels are naturally a concern for ITER, although recent SOLPS studies indicate that they may be tolerable for a somewhat reduced operational window, since volumetric power dissipation (mostly radiative) in the divertor can still reduce heat flux densities to acceptable levels, albeit at high neutral densities, maintaining the outer divertor leg partially detached [2]. On ITER at high performance, such partial detachment is mandatory if stationary heat fluxes are to be technologically manageable during baseline inductive burning plasma operation. The findings of this ITER simulation study are supported by results from N_2-seeding experiments at C-Mod, AUG and JET [20–22], where low Z impurity led to a reduction in the measured divertor peak heat fluxes by a factor 10–20 for acceptable performance in terms of core confinement. The λ_q for these experiments derived from the scaling presented here are: 1, 2.2 and 1.7 mm, for C-Mod, AUG and JET respectively. Thus, large reductions in target peak heat loads can be achieved despite very narrow values of λ_q at the lower end of the range in each device.

Returning to the discussion of estimating the integral power length for ITER (a composite of the exponential power fall-off length and the power spreading factor), as stated earlier, a sufficiently large value for S would lead to a situation in which the value of λ_q is of minor importance in determining λ_{int} at the divertor target. It seems plausible to assume that S will be at least in the same range as the values found in today's closed divertor tokamaks. In fact, the spreading could be considerably larger given the longer poloidal lengths from X-point to outer divertor target in ITER in comparison with smaller devices. For example, this length is five times larger on ITER than for AUG Divertor-IIb, where measurements found $S = 1.5$ mm. Ignoring such enhancement, even at $S = 1.5$ mm, $\lambda_{\mathrm{int,ITER}} \cong \lambda_{q,\mathrm{ITER}} + 1.64S \sim 3.5$ mm, for attached conditions (see also [24]). In addition to dedicated experiments varying the divertor leg geometries at DIII-D [25], existing SOLPS simulations [2, 11] and further code studies should also allow some light to be shed on the range of S which might be expected in different regimes on ITER.

Acknowledgments

The views and opinions expressed herein do not necessarily reflect those of the ITER Organization. This work was supported in part by the US DOE under DE-FC02-04ER54698 (GA), DE-AC02-09CH11466 (PPPL), DE-FC02-99ER54512 (MIT), DE-AC05-00OR22725 (ORNL), and DE-AC52-07NA27344 (LLNL). This work was supported by EURATOM and carried out within the framework of the European Fusion Development Agreement (EFDA). The views and opinions expressed herein do not necessarily reflect those of the European Commission.

References

[1] Progress in the ITER Physics Basis 2007 *Nucl. Fusion* **47** S203
[2] Kukushkin A.S. *et al* 2013 *J. Nucl. Mater.* **438** S203–7
[3] Pitts R.A. *et al* 2005 *J. Nucl. Mater.* **337–339** 146
[4] Eich T. *et al* 2007 *Plasma Phys. Control. Fusion* **49** 573
[5] Herrmann A. 2002 *Plasma Phys. Control. Fusion* **44** 883
[6] Eich T. *et al* 2011 *Phys. Rev. Lett.* **107** 215001
[7] Makowski M. 2012 *Phys. Plasmas* **19** 056122
[8] Fundamenski W. 2011 *Nucl. Fusion* **51** 083028
[9] Loarte A. *et al* 1999 *J. Nucl. Mater.* **266–269** 587
[10] Wagner F. 1985 *Nucl. Fusion* **25** 525
[11] Wischmeier M. *et al* 2011 *J. Nucl. Mater.* **415** S523
[12] LaBombard B. 2011 *Phys. Plasmas* **18** 056104
[13] Terry J.L. *et al* 2013 *J. Nucl. Mater.* **438** S212–5
[14] Gray T.K. *et al* 2011 *J. Nucl. Mater.* S **415** S360–4
[15] Eich T. *et al* 2013 *J. Nucl. Mater.* **438** S72–7
[16] Thornton A.J. *et al* 2013 *J. Nucl. Mater.* **438** S199–202
[17] Goldston R.J. 2012 *Nucl. Fusion* **52** 013009
[18] Kukuskin A. *et al* 2000 *Contrib. Plasma Phys.* **40** 233
[19] LaBombard B. 2008 *Phys. Plasmas* **15** 056106
[20] Snyder P.B. *et al* 2009 *Phys. Plasmas* **16** 056118
[21] Giroud C. *et al* 2012 *Nucl. Fusion* **52** 063022
[22] Kallenbach A. *et al* 2012 Multi-machine comparisons of divertor heat flux mitigation by radiative cooling with nitrogen *Proc. 24th IAEA Fusion Energy Conf. (San Diego, CA)* vol IAEA-CN-197, p ITR/P1-28 www-naweb.iaea.org/napc/physics/FEC/FEC2012/papers/345_ITRP128.pdf
[23] Loarte A. *et al* 2011 *Phys. Plasmas* **18** 056105
[24] Whyte D.G. *et al* 2013 *J. Nucl. Mater.* **438** S435–9
[25] Petrie T.W. *et al* 2013 *J. Nucl. Mater.* **438** S166–9
[26] LaBombard B. *et al* 2001 *Phys. Plasmas* **8** 3702
[27] Garcia O.E. *et al* 2007 *Nucl. Fusion* **47** 667
[28] Angioni C. *et al* 2009 *Plasma Phys. Control. Fusion* **51** 124017